Supporting Information

Photosensitized Reactive Chlorine Species-Mediated Therapeutic Destruction of Drug-Resistant Bacteria using Plasmonic Core-Shell Ag@AgCl Nanocubes as External Nanomedicines

Suresh Thangudu[1], Sagar Sunil Kulkarni[1], Raviraj Vankayala[2], Chi-Shiun Chiang[3], Kuo Chu Hwang[1*]

[1]Department of Chemistry, National Tsing Hua University, Hsinchu 30013, Taiwan, R.O.C.
[2] Department of Biosciences and Bioengineering, Indian Institute of Technology Jodhpur, Jodhpur, India
[3]Department of Biomedical Engineering and Environmental Sciences, National Tsing Hua University, Hsinchu 30013, Taiwan, R.O.C.
*E-mail: kchwang@mx.nthu.edu.tw

Estimation of Cl· radical concentration upon 532 nm light irradiation of Ag@AgCl NCs.

EPR measurements: For the detection of chlorine free radical (Cl·) using EPR, 50 μg/mL of Ag@AgCl nanostructures was dispersed in toluene and to this solution 0.1 M N-tert-butyl-α-phenylnitrone (PBN) spin trapping agent was added and then irradiated using 532 nm laser (250 mW/cm2, 10 min) under N_2 atmosphere with vigorous stirring. The photo-irradiated samples were then directly measured by using EPR at room temperature. Next to obtain the standard curve of chlorine radical generation, here we used different concentrations of carbon tetrachloride (CCl_4) and added the PBN spin trapping agent followed by irradiation with ultraviolet light (10 min irradiation at 222 nm wavelength, 53 mW/cm^2). Further the peak area vs concentration of standard concentration was plotted to get the standard calibration curve. Parameter settings: microwave power, 0.015 W; frequency, 9.8 GHz; time constant, 32.76 ms; scan width, 99.98 G.

To estimate the accurate concentration of chlorine free radical, here we followed the below calculations and the data shown in Figure S12.

Absorption cross section of carbon tetrachloride (CCl_4) at 228 nm is $4.85*10^{-20}$ cm^2 molecule^{-1}. [S1]

$$A(\lambda) = \sigma(\lambda) L[X]$$

A(λ)= A is the measured absorbance at wavelength λ

σ is the absorption cross section

L is the optical absorption path length, and [X] is the concentration of species X

Concentration of CCl_4 (M)	Absorption cross sections ($*10^{-20}$ cm^2 /atom)	Number of Cl· atoms ($*10^{22}$)	Conc. of Cl· free radicals (mmol)
10.37	4.85	0.5626	9.3417
6.89	3.222	0.3737	6.2060
3.445	1.6112	0.1869	3.1033
1.378	0.6444	0.07475	1.2412
0.0275	0.0128	0.00148	0.02465

Neat CCl_4 (1 mL) was irradiated for 10 min under light. Light intensity on sample is 53 mW/cm^2 @222 ± 5 nm.

$$N_{incident} = \frac{Pt\lambda}{hc}$$

h= Planck's constant, c= light velocity, λ= wavelength, *t* is time (1h=3600 s)

$$N_{incident} = \frac{Pt\lambda}{hc} = \frac{53.0 * 10^{-3}\, W * 600\, sec * \left(222 * 10^{-9}\right) m}{6.63 * 10^{-34}\, j.sec * 3 * 10^{8}\, m/sec}$$

$$= 3.5493 * 10^{19}$$

Total no. of photons absorbed by sample

$$N_{total} = N_{incident} * Atomic\ density * \sigma * dx$$

σ is the cross section, ρ is density and dx is the thickness

$$N_{total} = 3.5493 * 10^{19} * \frac{\rho * N_A\ \ atoms}{M.Wt\quad cm3} * 4.85 * 10^{-20}\, \frac{cm2}{atom}\ * 1.5\ cm$$

$$N_{total} = 3.5493 * 10^{19} * \frac{1.59 * 6.023 * 10^{23}}{153.82}\left(\frac{atoms}{cm3}\right) * 4.85 * 10^{-20}\, \frac{cm2}{atom}\ * 1.5\ cm$$

$$N_{total} = 1.6075 * 10^{22}$$

Quantum yield (QY) for the generation of Cl. radical by 222 nm UV light irradiation of CCl_4 is known to be 0.35.[S2] [*ref; J. Chem. Sci.* 2006, *118 (4) 341–344*]

$$QY = \frac{Number\ of\ cl.}{N_{Total}}$$

$$\textbf{Number of Cl}^{\cdot} \textbf{ = QY * N}_{\textbf{Total}}$$

$$= 0.35 * 1.6075 * 10^{22}$$

$$\text{Number of Cl}^{\cdot} \text{ atoms} = 0.5626 * 10^{22}$$

The quantity (in moles) of chlorine atoms = number of $Cl^{\cdot}$ atoms/ Avogadro number

$$= 0.5626 * 10^{22} / 6.023 * 10^{23}$$

$$= 0.00934 \text{ moles}$$

Estimated transient Cl. radical concentration generated from Ag@AgCl NCs (@ 50 μg/mL, 0.75 mL) under 532 nm light irradiation (10 min irradiation, 250 mW/cm^2, EPR peak area is 130000) is 2.65 mmoles, which is corresponding to a transient $Cl^{\cdot}$ radical concentration of 0.0588 μM within 10 μsec time interval.

Table S1. A brief literature overview of various examples of light activatable nanomaterials mediating *in vivo* therapeutic effects in treating bacterial infections.

S. No.	Nanomaterial	Bacteria	Inactivation pathway	Conditions	Ref.
1	Ag@AgCl NCs	MRSA, E.coli	Chlorine free radicals	532 nm, 10 min, 250 mW/cm^2	**Present work**
2	SiO_2-Cy-Van	MRSA	PTT	808 nm, 5 min, 1.5 W/cm^2	[S3]
3	OC-UCNP-ZnPc	MRSA	PDT	980 nm, 15 min, 0.4 W/cm^2	[S4]
4	Ach@RuNPs	MRSA	PTT/PDT	808 nm, 15 min, 1.0 W/cm^2	[S5]
5	AuAg	MRSA	Silver ions	-	[S6]
6	PEG-MoS_2 NFs	Amplicin resistant E.coli	PTT/PDT	808 nm, 10 min, 1.0 W/cm^2	[S7]
7	(Ag+-GCS-PDA@GNRs)	MRSA	PTT	808 nm, 7 min, 0.5 W/cm^2	[S8]
8	QA-Au NCs	MRSA	Electrostatic interaction	-	[S9]
9	MoS_2-BNN6	Amplicin resistant E.coli	PTT + NO release	808 nm, 10 min, 0.5 W/cm^2	[S10]
10	MoS_2-PDA-Ag	S. aureus	PTT	785 nm, 10 min, 0.5 W/cm^2	[S11]

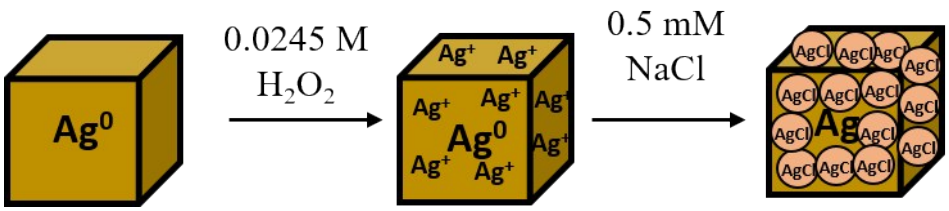

Scheme S1. Schematic representation of Ag@AgCl NCs formations via insitu oxidation process.

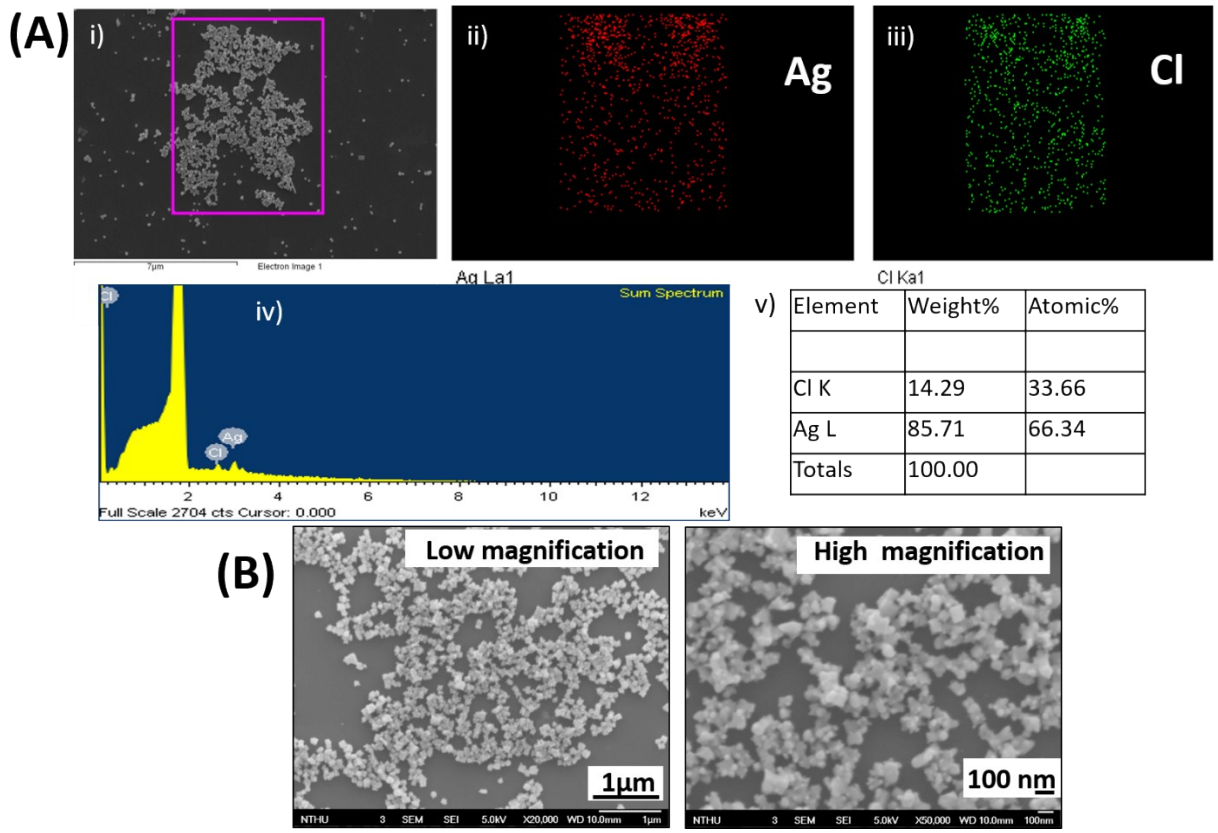

Figure S1. (A) Energy Dispersive Spectroscopy (EDS) analysis and (B) Low and high magnification SEM images of Ag@AgCl NCs.

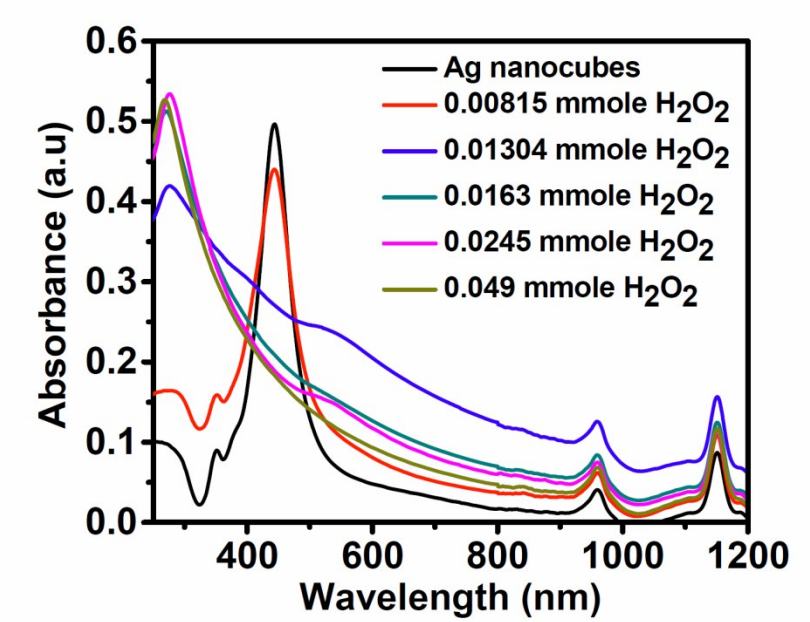

Figure S2. Formation of plasmonic Ag@AgCl NCs monitored by UV-visible-NIR absorption spectra upon varying the concentrations of an oxidant, H_2O_2, in the reaction solution.

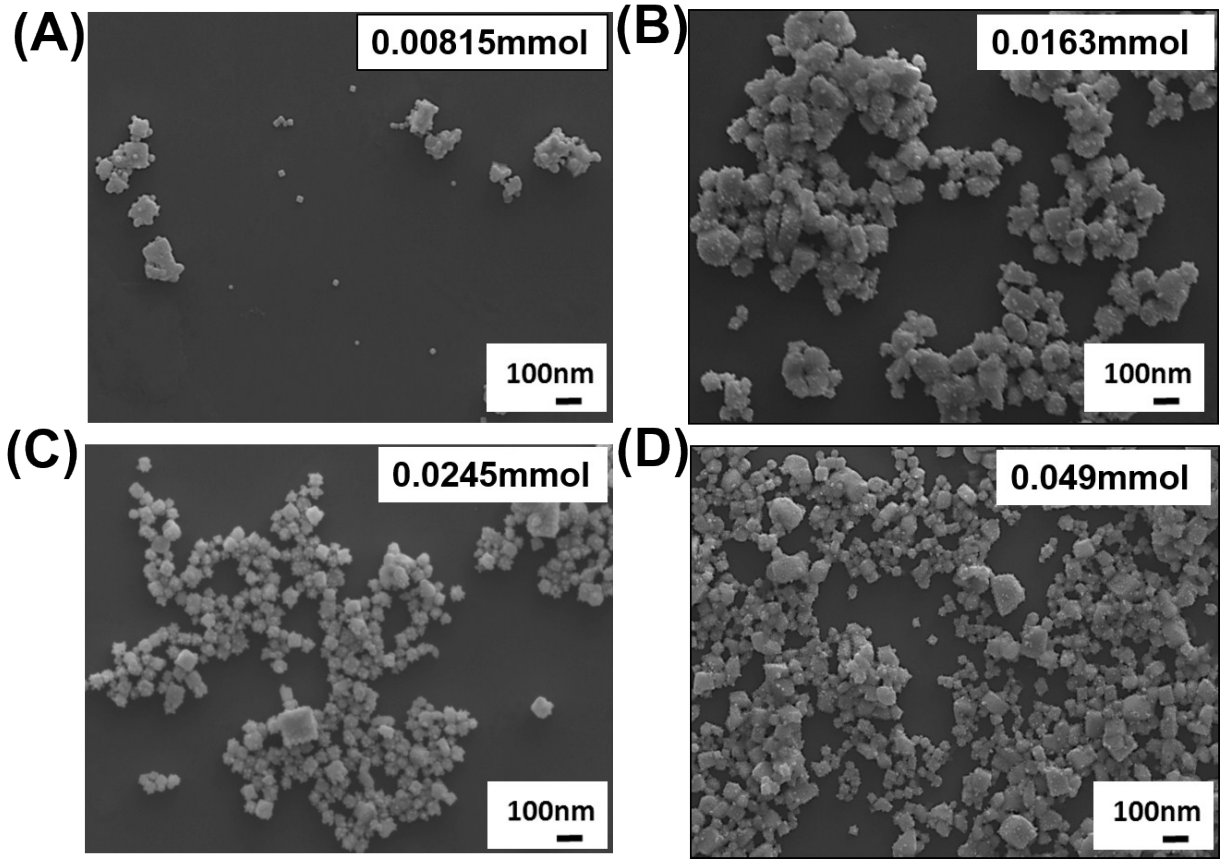

Figure S3. Effect of oxidant (H_2O_2) concentration on oxidation of Ag NCs to form Ag@AgCl NCs. The morphologies of Ag@AgCl NCs were presented vs. the H_2O_2 concentration. (Experimental condition: Ag NCs (optical density is 2.3) oxidized by H_2O_2 of different concentrations in the presence of 0.5 mM NaCl in an aqueous solution.

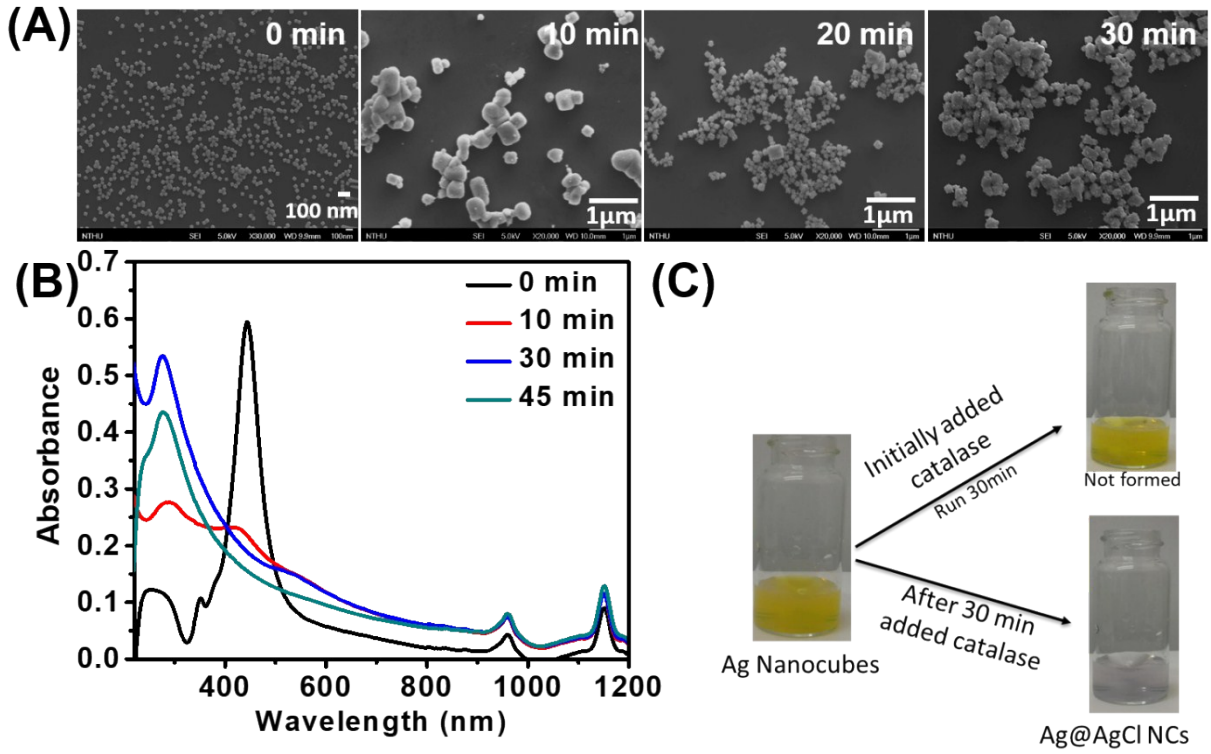

Figure S4. (A) SEM, and (B) UV-visible-NIR absorption spectra of reaction solution at different time intervals, and (C) optical images of the reaction solution before and after 30 min with the addition of catalase (100 µL of 0.3 mg/L).

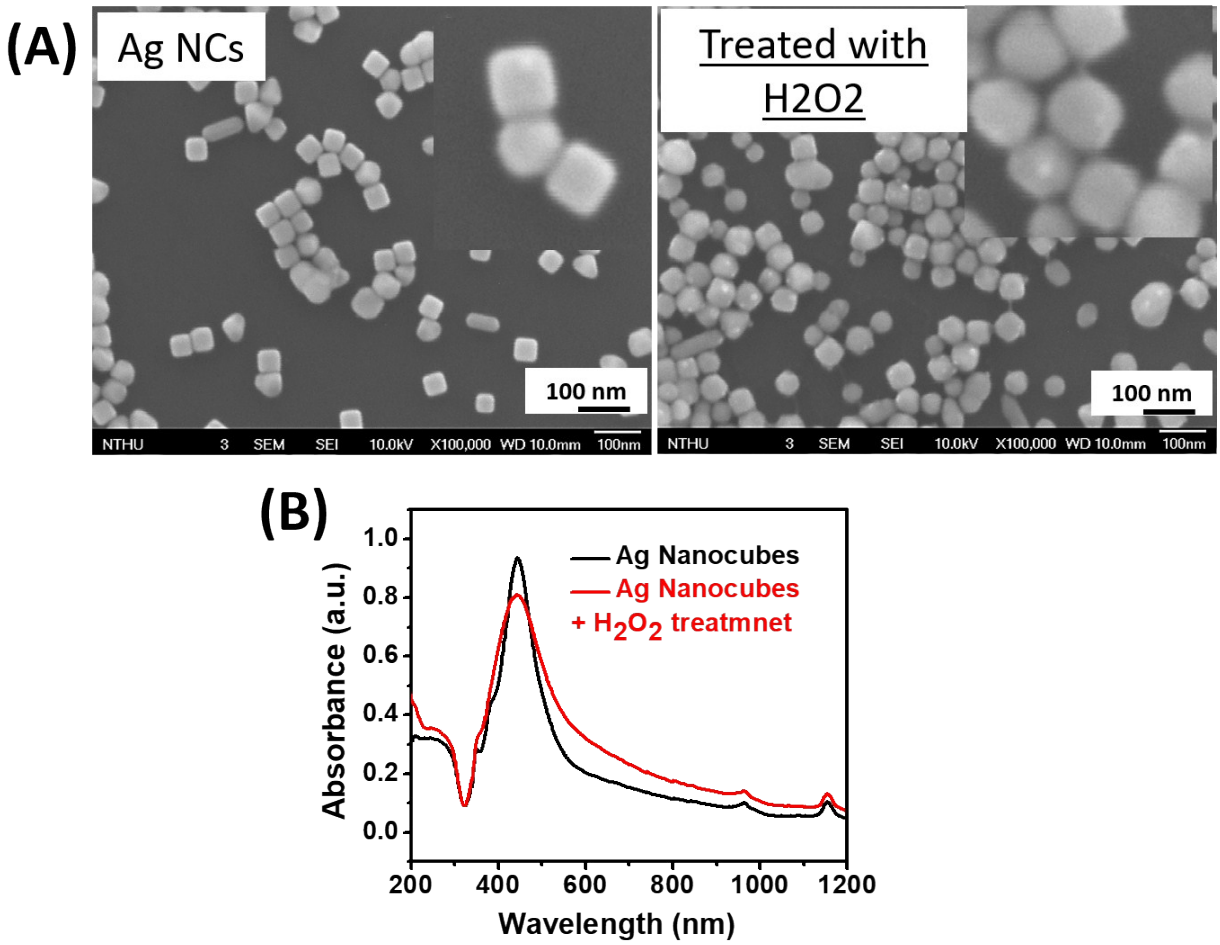

Figure S5. (A) and (B) represent the SEM images, and (C) UV-vis-NIR absorption spectra of Ag NCs before and after treatment with H_2O_2 (in the absence of NaCl), respectively.

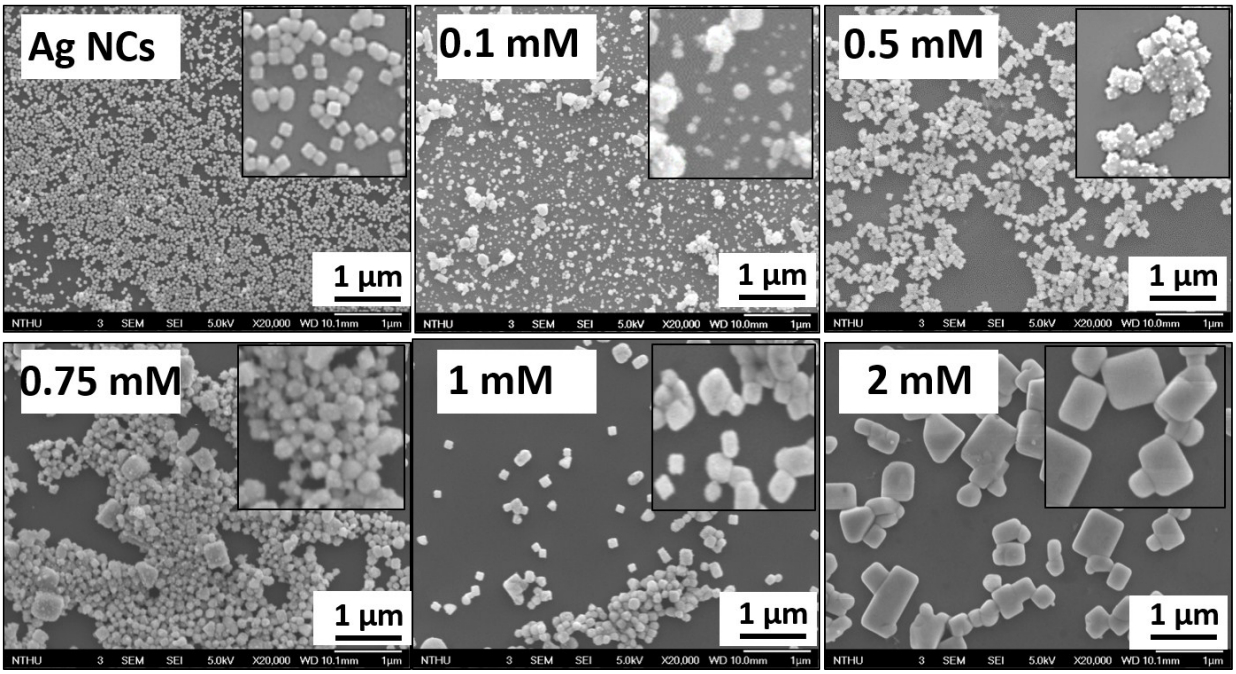

Figure S6. SEM images of plasmonic Ag@AgCl NCs with different sizes. The sizes of Ag@AgCl NCs were tuned by varying the concentrations of NaCl (as labeled in the figure) in the solution during the preparation of Ag@AgCl NCs.

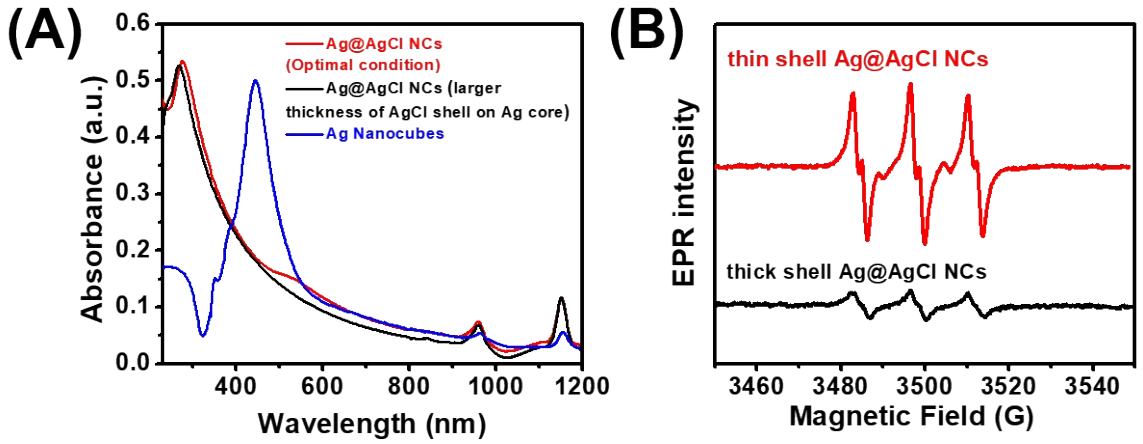

Figure S7. (A) UV-vis-NIR absorption of Ag@AgCl NCs with different sizes, and (B) EPR spectra of Cl. radicals generated by photo-excitation of Ag@AgCl NCs of different shell thickness. (experimental condition: 1 mg/mL of NCs in toluene solution, 0.1 M PBN spin trapping probe, 532 nm light irradiation for 10 min, 250 mW/cm^2).

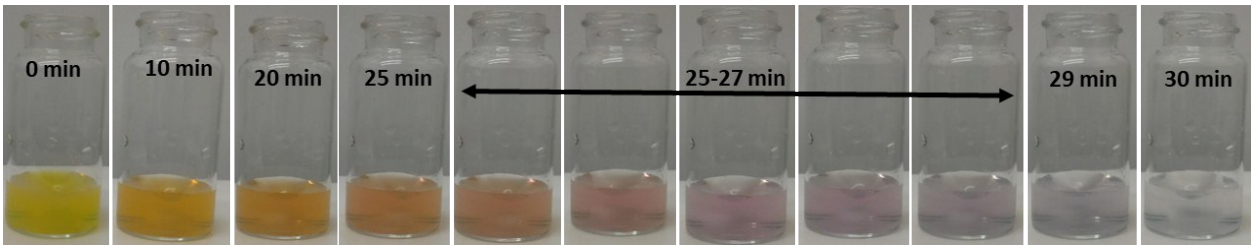

Figure S8. Optical images of the reaction solutions during the oxidation process taken at different time intervals as indicated in the figure.

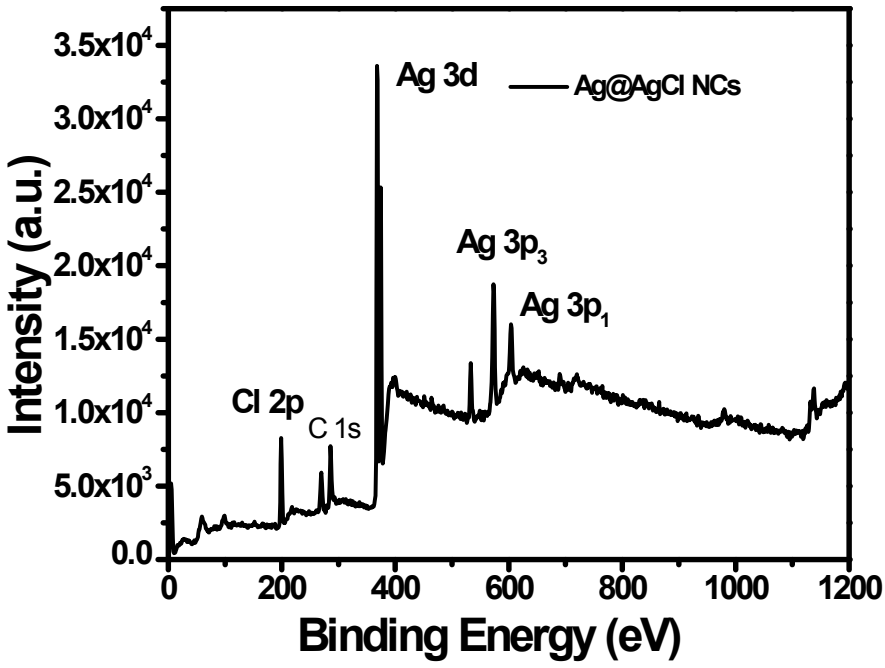

Figure S9. XPS survey spectrum of Ag@AgCl nanocrystals.

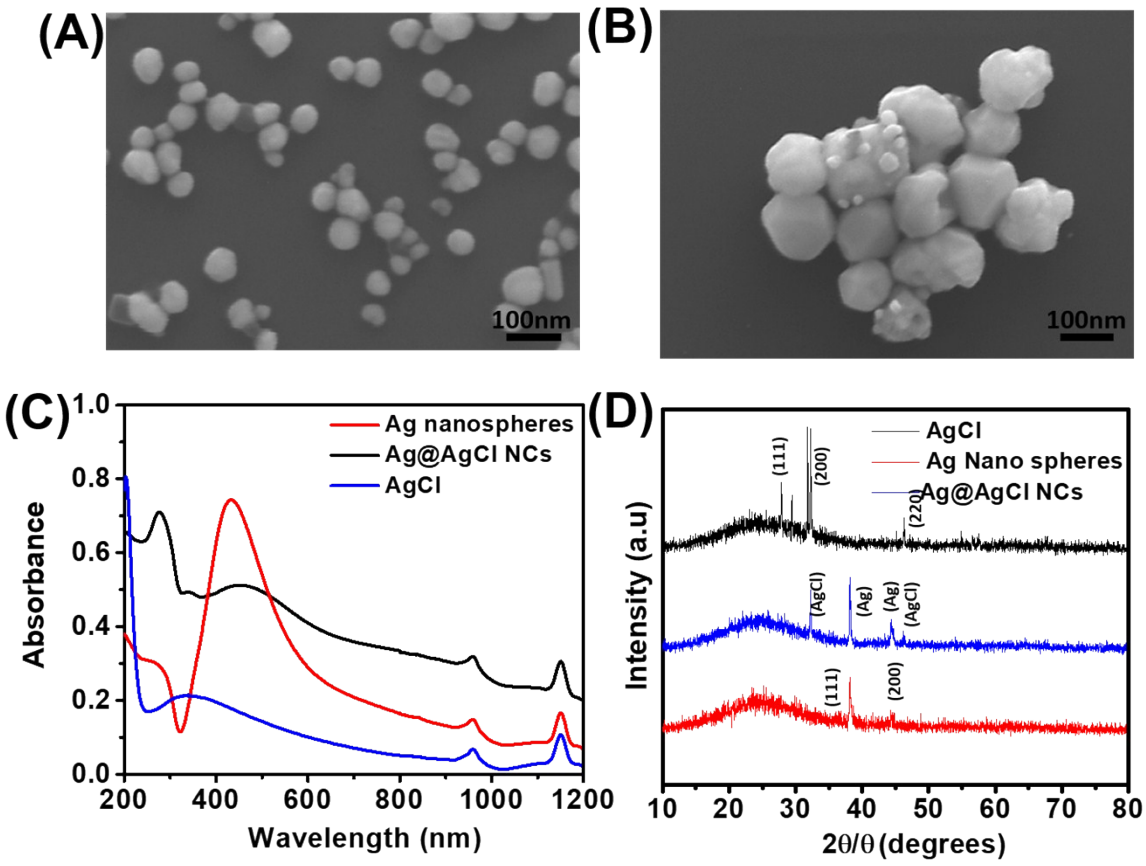

Figure S10. Synthesis of Ag@AgCl NCs using Ag nanospheres as template. (A) and (B) represent SEM images of Ag nanospheres and Ag@AgCl NCs. (C) UV-vis-NIR absorption spectra and (D) XRD of Ag nanospheres, AgCl and Ag@AgCl NCs.

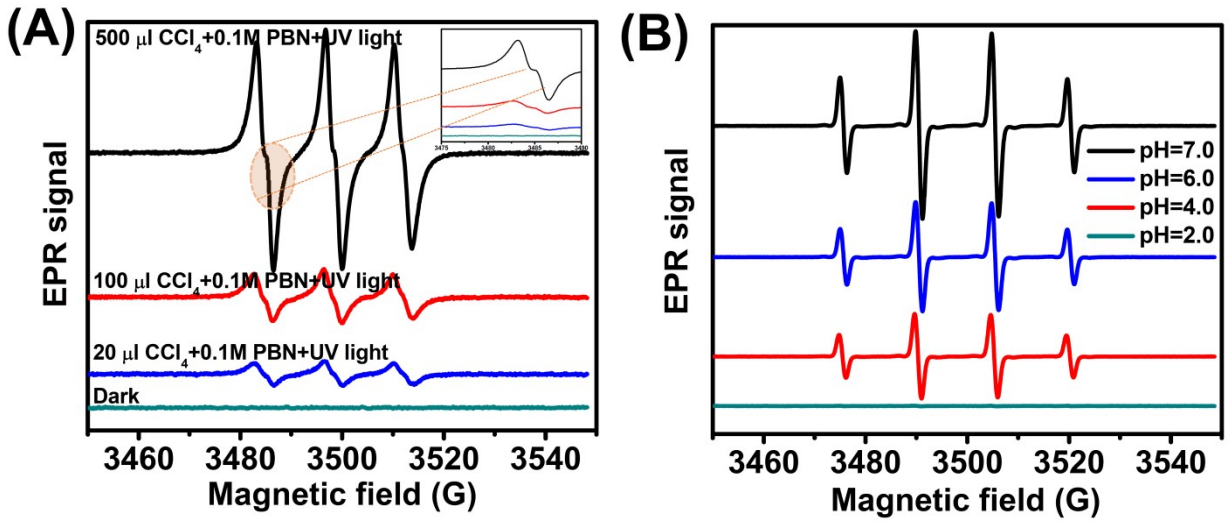

Figure S11. (A) EPR spectra of chlorine radical generated from carbon tetrachloride under uv light exposure (100 W high pressure Hg lamp with UV filter; 20 mW/cm^2; 10 min), and (B) hydroxyl radical generation from Ag@AgCl NCs (50 μg/mL) at different pH conditions under 532 nm laser (250 mW/cm^2,10 min) irradiation.

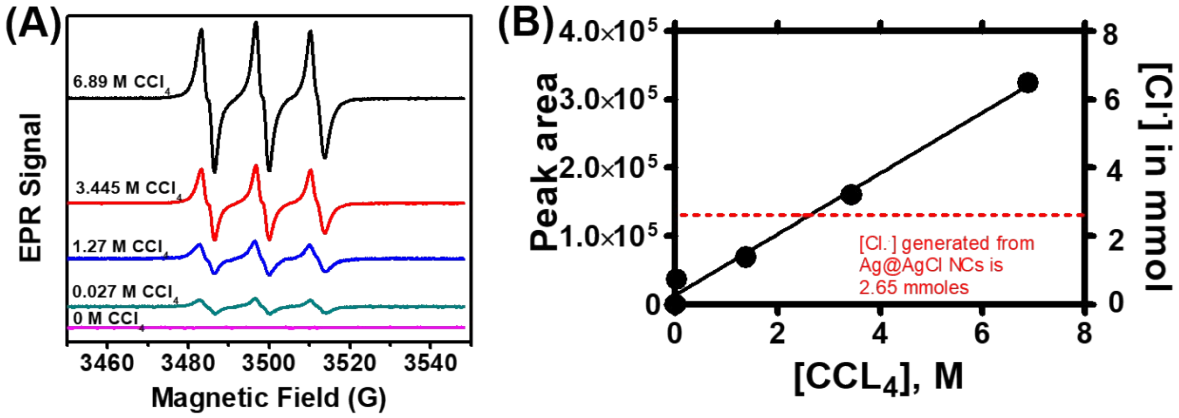

Figure S12. (A) EPR intensities of Cl. radicals generated by UV (222 nm, 53 mW/cm^2) irradiation of different CCl_4 concentrations in toluene. The Cl. radical trapping agent is 0.1 M N-tert-butyl-α-phenylnitrone (PBN) in toluene. (b) EPR signal intensities were plotted as a function of the CCl_4 concentrations. By knowing the incident light intensity, photo irradiation time, and the quantum yields of Cl· radical generation from CCl_4, the Cl· radical concentrations (or quantities) can be calculated from the EPR signal intensities.

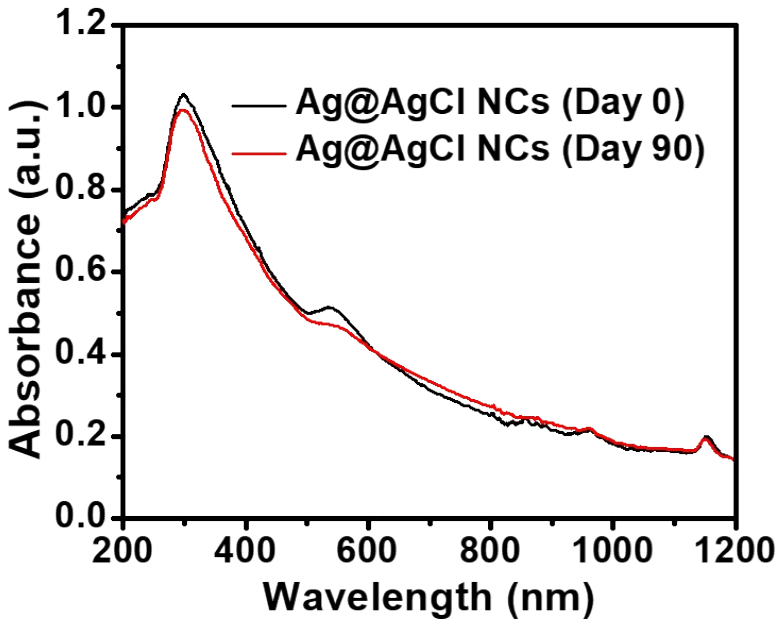

Figure S13: Optical stabilities of freshly synthesized Ag@AgCl NCs at day 0 (black) and after 90 days (red line) of storage at room temperature.

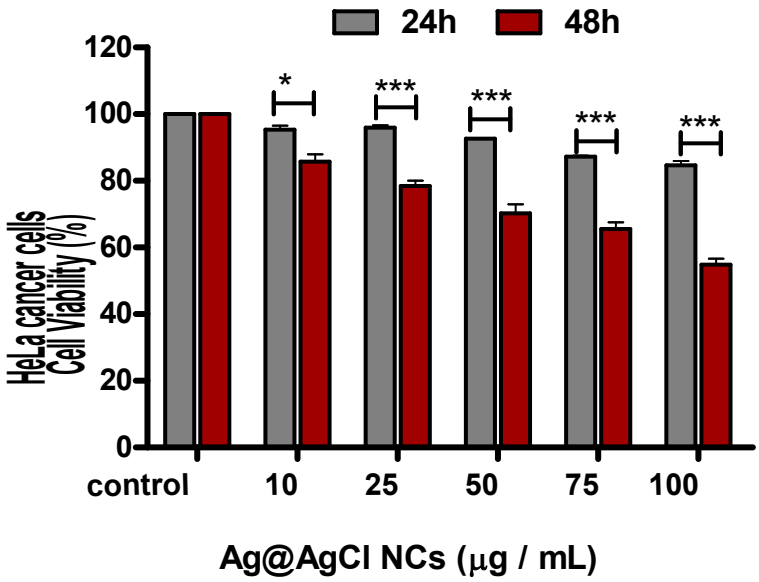

Figure S14. Cytotoxicity of Ag@AgCl NCs in HeLa cells at different incubation periods. Statistical analysis was performed using one-way ANNOVA with $^{**}p < 0.01$ and $^{***}p < 0.001$, respectively. The error bars represent the standard deviation of three repeations of experiments.

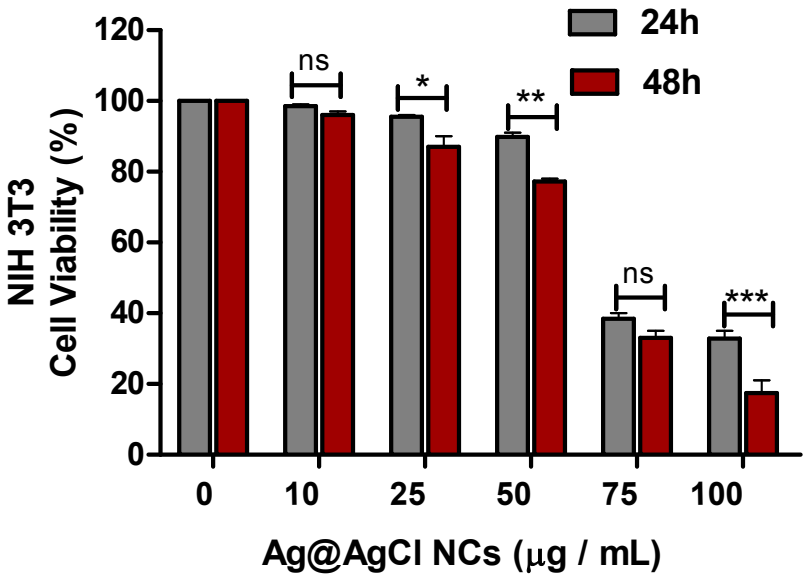

Figure S15. Cytotoxicity of Ag@AgCl NCs in mouse fibroblast cells (NIH3T3) under dark at 24 and 48 h incubation time, respectively. Asterisks indicate the statistical significance between the indicated pairs (*$p < 0.05$). The error bars represent the standard deviation of three repeations of experiments.

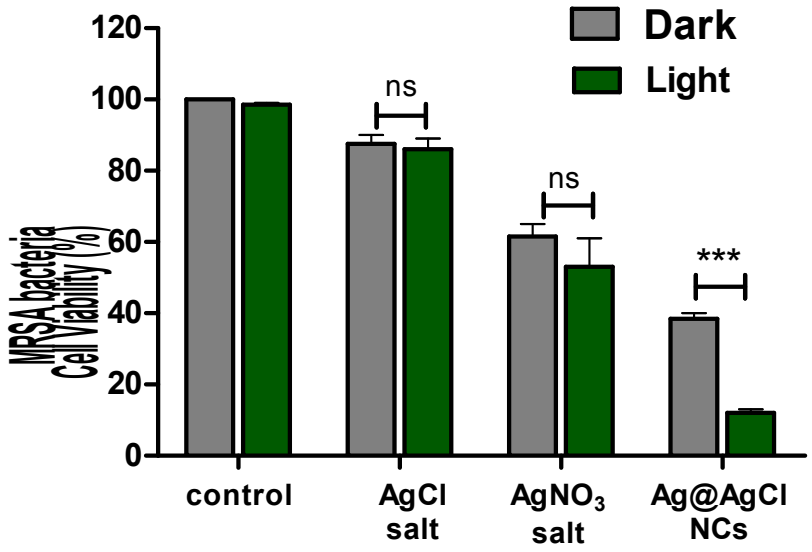

Figure S16. Comparison of antibacterial activities of silver salts, including AgCl (commercial microparticles), $AgNO_3$, and Ag@AgCl NCs. The concentrations are all the same, 50 μg/mL, for all three silver salts. The laser light source is 532 nm, 250 mW/cm^2, 10 min. The error bars represent the standard deviation of three repeations of experiments.

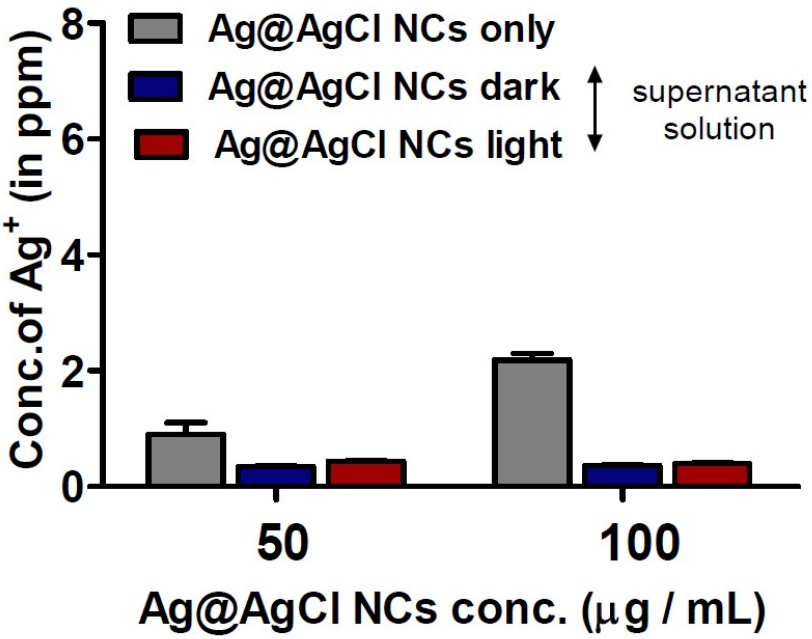

Figure S17. ICP-MS analysis of the supernatant from a solution containing Ag@AgCl NCs in dark and photo-irradiation (532 nm, 250 mW/cm^2, 10 min) conditions, respectively. The error bars represent the standard deviation of three repeations of each experiment.

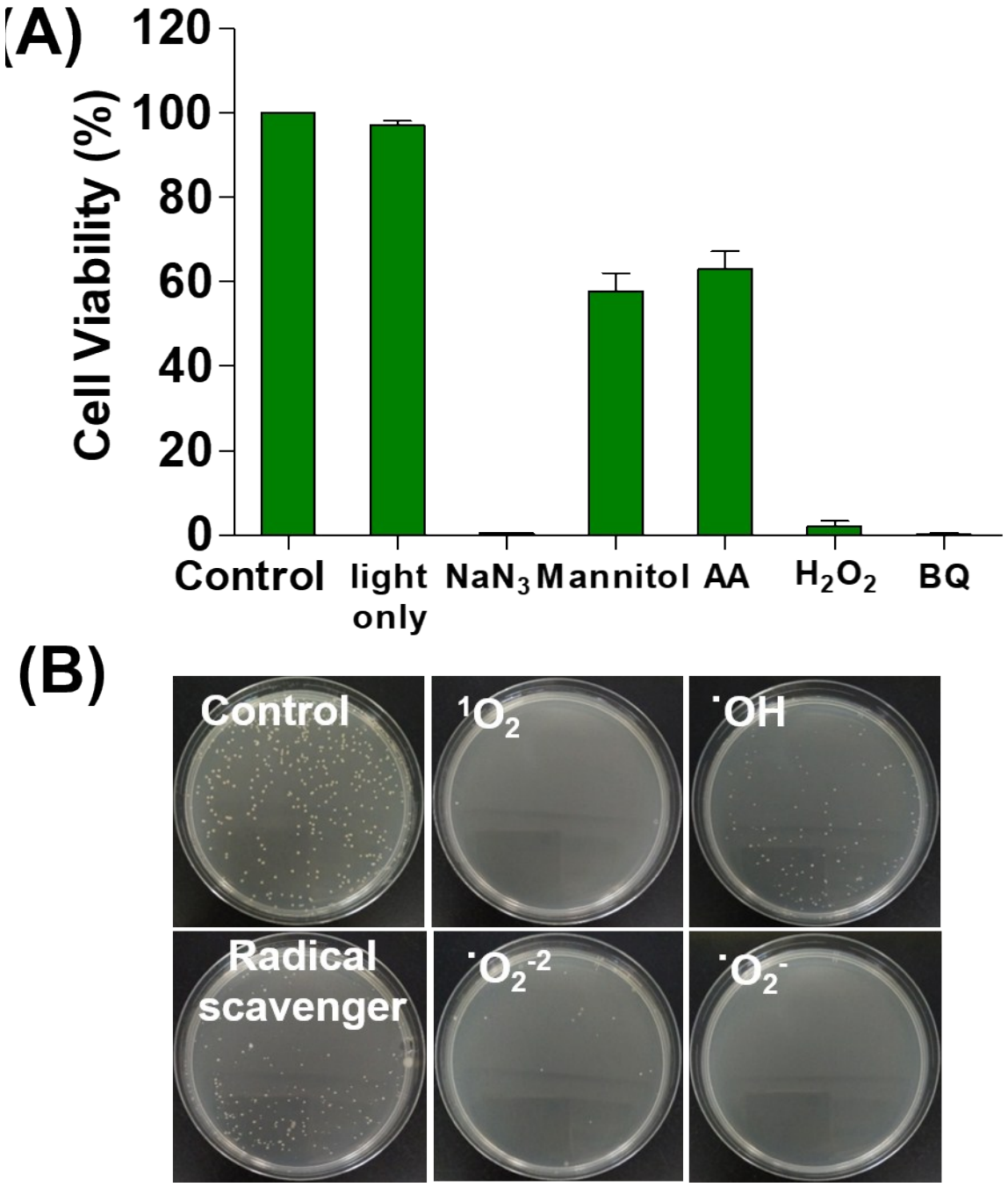

Figure S18. Photocatalytic inactivation of MRSA bacteria using Ag@AgCl NCs in the presence of various scavangers. The concentration of scavengers are 0.05 mmol/L at 50 μg/mL of Ag@AgCl NCs (532 nm laser; 10 min; 250 mW/cm^2). The error bars represent the standard deviation of three repeations of experiments.

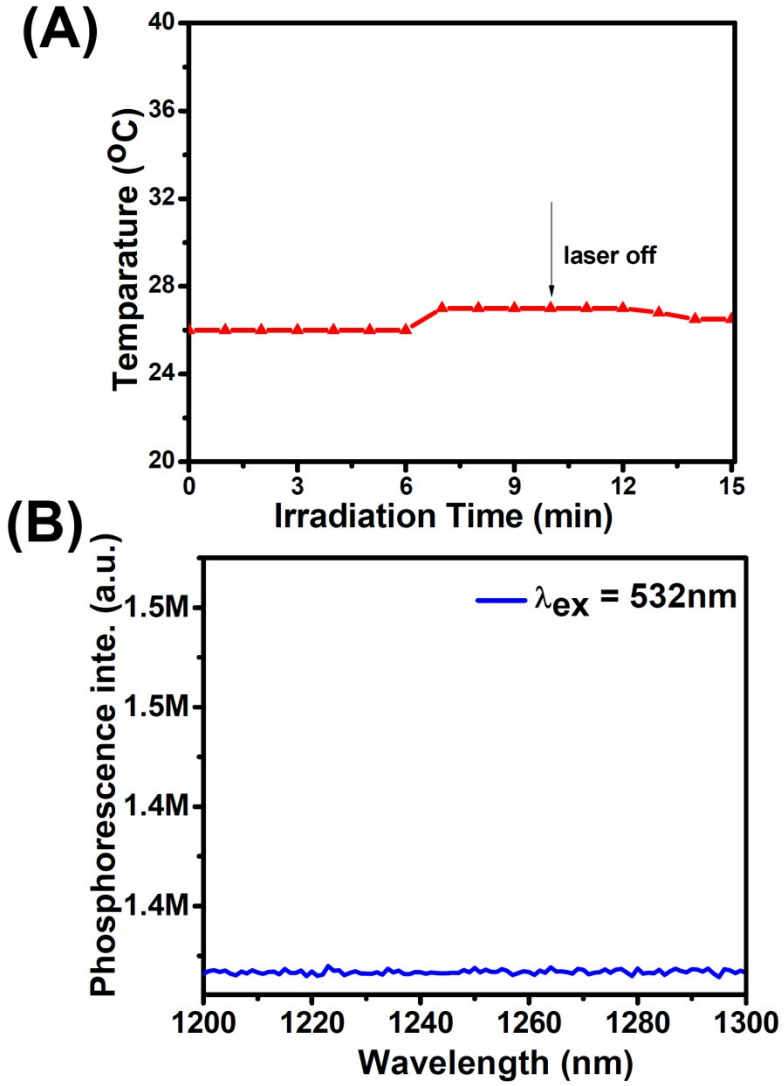

Figure S19. (A) Photothermal temperature rise profile from a Ag@AgCl NCs (1 mg/mL) aqueous solution. The laser light source is 532 nm, 250 mW/cm^2, 10 min irradiation. (B) singlet oxygen phosphorescence emission spectra of Ag@AgCl NCs at 532 nm excitation.

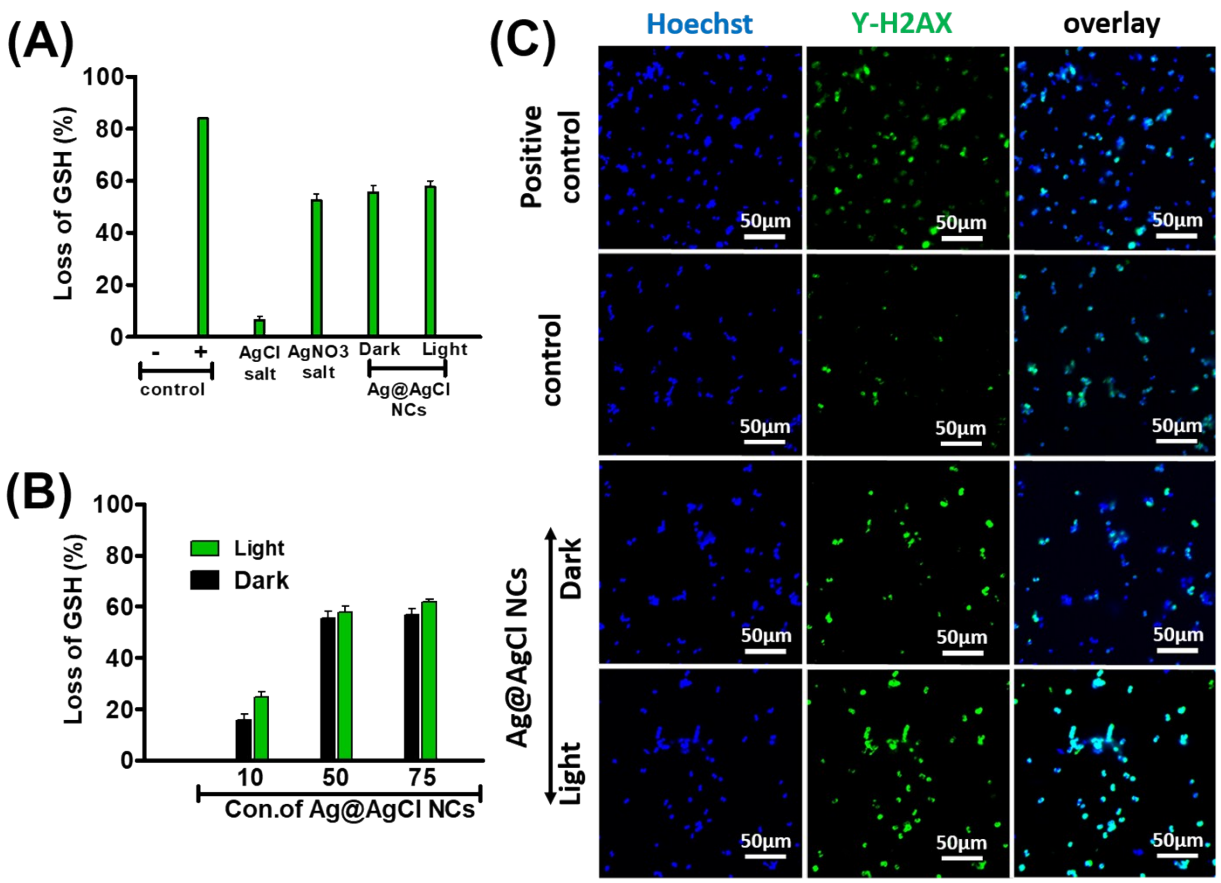

Figure S20. *Mechanistic investigation of photocatalytic inactivation of bacteria mediated by Ag@AgCl NCs.* (A) The extent of loss of GSH in MRSA bacteria after 1 h incubation with AgCl (microparticles from commercial sources), $AgNO_3$ and Ag@AgCl NCs (bacteria without having silver salts or NCs treatment were used as negative control, H_2O_2 was used as a positive control (50 μL, 30% H_2O_2)). (B) Loss of GSH under dark and light by varying the concentration of Ag@AgCl NCs. (C) Direct observation of DNA damage of MRSA bacteria subjected to the different treatment groups (DNA phorporylation agent γH2AX (green), nucleus stain Hoechst (blue), H_2O_2 was used as a positive control (50 μL, 30% H_2O_2). The concentrations of AgCl, $AgNO_3$ and Ag@AgCL NCs are the same, 50 μg/mL. The output of a 532 nm laser (250 mW/cm^2, 10 min) was used as the light source. The error bars represent the standard deviation of three repeations of experiments.

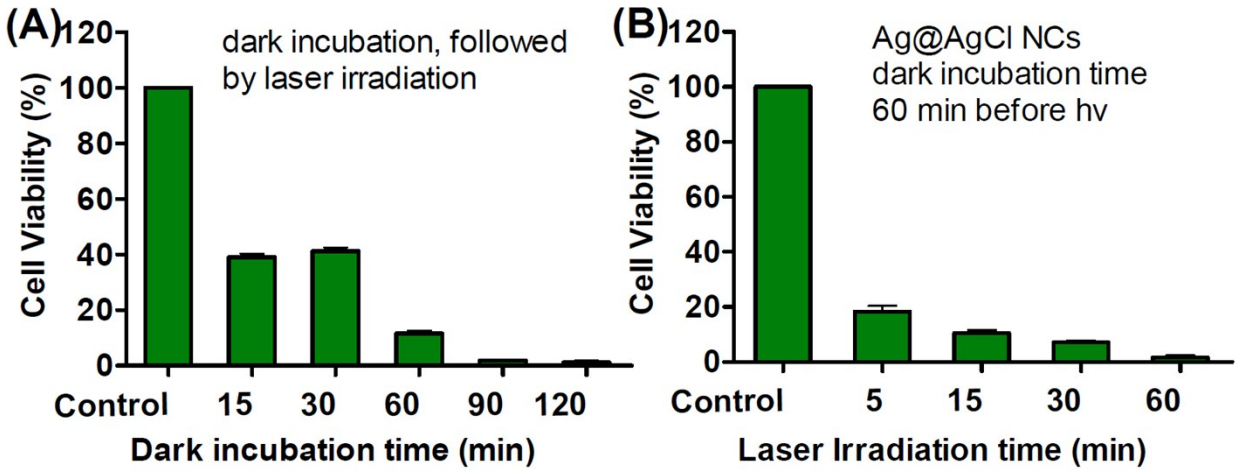

Figure S21. Photocatalytic inactivation of MRSA at different (A) dark incubation time of Ag@AgCl NCs (at a dose of 50 μg/mL) with bacteria before laser irradiation (532 nm laser; 250 mW/cm^2; 10 min); and (B) cell viability as a function of laser irradiation time. The bacteria was incubated with 50 μg/mL Ag@AgCl NCs for 60 min before laser irradiation. In the control experiment, no Ag@AgCl NCs was added to the bacteria solution and the time point is at 0 min. The error bars represent the standard deviation of three repeations of experiments.

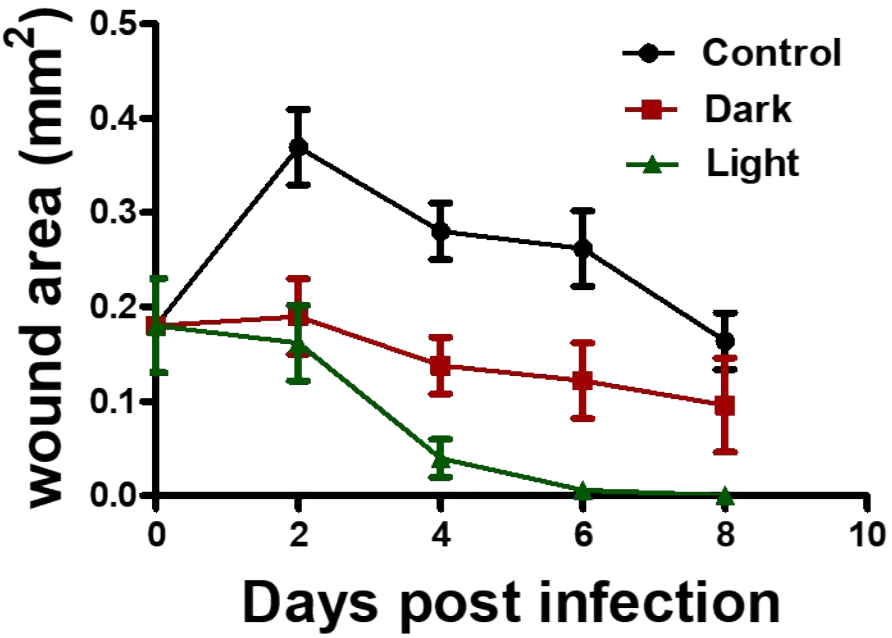

Figure S22. Estimated infected wound area of the mice subjected to various treatments monitored as a function of days post infection. The error bars represent the standard deviation of three experiments.

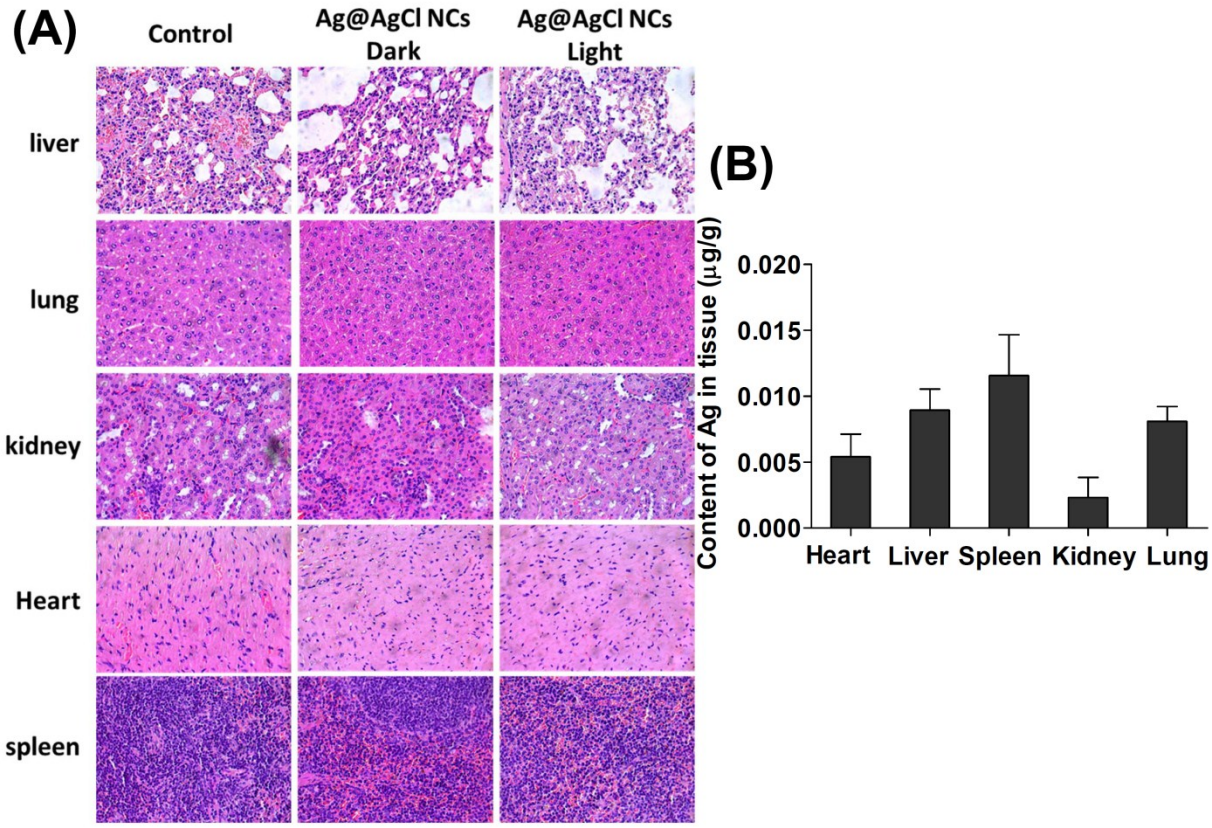

Figure S23. (A) H&E staining analysis and (B) content of silver in the tissue for all major organs after 8 days of treatment. The error bars represent the standard deviation of three experiments.

Supporting References

[S1]. N. R. Carlon, D. K. Papanastasiou, E. L. Fleming, C. H. Jackman, P. A. Newman, J. B. Burkholder, *Atmos. Chem. Phys*., 2010, **10**, 6137.

[S2]. M. Tak, M. Chandra, D. Senapati, *J Chem. Sci.,* 2006, **118**, 341.

[S3]. Z. Zhao, R. Yan, X. Yi, J. Li, J. Rao, Z. Guo, Y. Yang, W. Li, Y.-Q. Li, C. Chen, *ACS Nano,* 2017, **11**, 4428.

[S4]. S. Li, S. Cui, D. Yin, Q. Zhu, Y. Ma, Z. Qian, Y. Gu, *Nanoscale,* 2017, **9**, 3912.

[S5]. X. Huang, G. Chen, J. Pan, X. Chen, N. Huang, X. Wang, J. Liu, *J. Mater. Chem. B,* 2016, **4**, 6258.

[S6]. T. Kim, Q. Zhang, J. Li, L. Zhang, J. V. Jokerst, *ACS Nano,* 2018, **12**, 5615.

[S7]. W. Yin, J. Yu, F. Lv, L. Yan, L. R. Zheng, Z. Gu, Y. Zhao, *ACS Nano,* 2016, **10**, 11000.

[S8]. M. Liu, D. He, T. Yang, W. Liu, L. Mao, Y. Zhu, J. Wu, G. Luo, J. Deng, *J. Nanobiotechnology,* 2018, **16**, 23.

[S9]. Y. Xie, Y. Liu, J. Yang, Y. Liu, F. Hu, K. Zhu, X. Jiang, *Angew. Chem. Int. Ed.,* 2018, **57**, 3958.

[S10]. Q. Gao, X. Zhang, W. Yin, D. Ma, C. Xie, L. Zheng, X. Dong, L. Mei, J. Yu, C. Wang, Z. Gu, Y. Zhao, *Small,* 2018, **14**, 1802290.

[S11]. L. Yuwen, Y. Sun, G. Tan, W. Xiu, Y. Zhang, L. Weng, Z. Teng, L.Wang, *Nanoscale,* 2018, **10**, 16711.